Letter

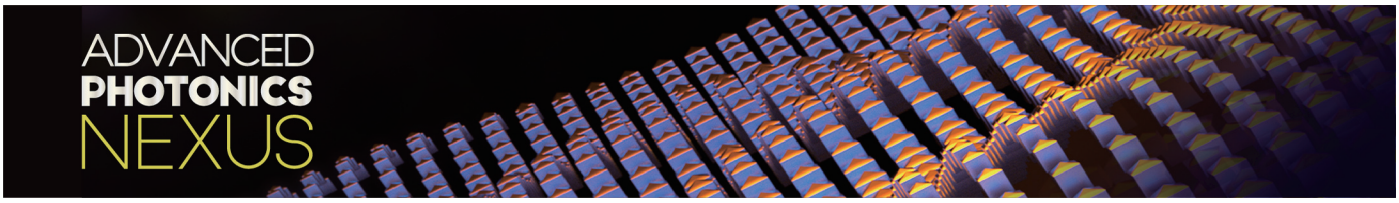

Vortex-induced quasi-shear polaritons

Shuwen Xue,† **Yali Zeng**,† **Sicen Tao, Tao Hou, Shan Zhu, Chuanjie Hu, and Huanyang Chen***
Xiamen University, Institute of Electromagnetics and Acoustics, College of Physical Science and Technology, Department of Physics, Xiamen, China

Abstract. Hyperbolic shear polaritons (HShPs) emerge with widespread attention as a class of polariton modes with broken symmetry due to shear lattices. We find a mechanism of generating quasi-HShPs(q-HShPs). When utilizing vortex waves as excitation sources of hyperbolic materials without off-diagonal elements, q-HShPs will appear. In addition, these asymmetric q-HShPs can be recovered as symmetric modes away from the source, with a critical transition mode between the left-skewed and right-skewed q-HShPs, via tuning the magnitude of the off-diagonal imaginary component and controlling the topological charge of the vortex source. It is worth mentioning that we explore the influence of parity of topological charges on the field distribution and demonstrate these exotic phenomena from numerical and analytical perspectives. Our results will promote opportunities for both q-HShPs and vortex waves, widening the horizon for various hyperbolic materials based on vortex sources and offering a degree of freedom to control various kinds of polaritons.

Keywords: hyperbolic shear polaritons; vortex waves; off-diagonal imaginary component; scaling factor; topological charge.

Received Sep. 16, 2022; revised manuscript received Oct. 13, 2022; accepted for publication Dec. 15, 2022; published online Jan. 3, 2023.

[DOI: 10.1117/1.APN.2.1.015001]

1 Introduction

Polaritons are half-light and half-matter quasi-particles formed by the interaction between light and matter modes involving collective oscillations of polarization charges in matter, enabling nanoscale control of light. Traditional surface plasmon polaritons are electromagnetic waves that travel along the metal–dielectric interface, which have received a great deal of attention.[1–4] In addition, exhibiting long lifetimes and low optical losses, phonon polaritons (PhPs) emerge as an important substitute for plasmonic counterparts in subdiffraction light–matter interaction and nanophotonic applications[5,6], such as the PhPs in polar van der Waals materials including hexagonal boron nitride[7–9], α-phase molybdenum oxide (α-MoO_3),[10–13] and so on. Remarkably, α-MoO_3, capable of supporting topological transitions, enables both inplane hyperbolic and elliptical PhPs.[14] Furthermore, a new polariton class in low-symmetry monoclinic and triclinic crystals (e.g., β-phase Ga_2O_3) called hyperbolic shear polaritons (HShPs) complements the previous observations of hyperbolic PhPs and exists when the dielectric tensor is not diagonalized.[15] This drives us to consider the possibility of the generation of HShPs in orthogonal systems (with three major polarizability axes) without off-diagonal elements.

As mentioned earlier, PhPs with long lifetimes and low optical losses offer more opportunities for infrared nanophotonic applications. Yet, most methods of stimulating PhPs are based on a simple dipole source and it is high time to take complex structured fields into account. The vortex as a representative complex structured field, not only exists in nature, such as spiral galaxies in the Milky Way and typhoon vortices, but also is extensively applied in structured electromagnetic and optical fields. The optical vortex is a beam of photons that propagates with singularity on its axis in the form of $e^{im\theta}$, where m and θ represent the topological charge and azimuth angle, respectively. Compared with the conventional plane wave or dipole source, vortex beams with a higher degree of freedom attract enormous applications and interest, including vortex tweezers,[16,17] high-capacity optical communications,[18] optical microscopy imaging,[19,20] nonlinear optics,[21,22] and polaritonic vortices.[23,24] Here, we intend to combine a vortex with PhPs and study the propagation characteristics of the vortex in anisotropic materials (or even hyperbolic materials).

In this letter, based on the motivations mentioned above, we propose an approach to induce quasi-HShPs (q-HShPs) in orthogonal systems without off-diagonal elements and study

*Address all correspondence to Huanyang Chen, kenyon@xmu.edu.cn
†These authors contributed equally to this letter.

the propagation characteristics of vortex waves as excitation sources in hyperbolic materials. In detail, asymmetric q-HShPs will occur when the vortex waves are used as excitation sources of hyperbolic materials, providing a new degree of freedom to control various polaritons. More interestingly, asymmetric q-HShPs (left-skewed and right-skewed q-HShPs) excited by the vortex source can be recovered as symmetric modes by regulating the magnitude of the off-diagonal imaginary component, arising from the critical symmetry transition. We verify these unique phenomena theoretically and numerically, providing a platform for future research of HShPs and vortex waves.

2 Results and Discussion

The diagram in Fig. 1 illustrates the simulated magnetic fields (H_z), the corresponding intensities ($|H|$), and the fast Fourier transform (FFT (Re[H_z])) of a vortex wave with different topological charges ($m = 0, \pm 1$) as the excitation source of hyperbolic materials at 718 cm^{-1}, where the simulated permittivity tensor is obtained by diagonalizing the real part of the permittivity tensor of β-phase Ga_2O_3 (Re[$\varepsilon(\omega)$]) individually at each frequency. Here, the off-diagonal permittivity tensor elements are set as zero, and the corresponding material parameters (ε_{uu} and ε_{vv}) are achieved from Ref. 13. For the conventional point source ($m = 0$), the simulated field expresses hyperbolic feature and symmetry, as shown in Fig. 1(b). On the contrary, if utilizing vortex wave as excitation sources ($m = \pm 1$), the simulated magnetic field tips to one side [Figs. 1(a) and 1(c)], obviously presenting an asymmetric phenomenon. For the opposite topological charges $m = \pm 1$, the simulated magnetic fields tip to the left side if $m = -1$ while they tip to the right side if $m = +1$. The corresponding intensities ($|H|$) and FFT dispersions are displayed in Figs. 1(d)–1(i), which tip in opposite directions for opposite topological charges, as we predicted before. Therefore, the asymmetric q-HShPs appear when vortex waves serve as excitation sources of hyperbolic materials, validating the possibility of generating asymmetric q-HShPs in orthogonal systems without off-diagonal elements. The simulated fields are obtained with finite-element software COMSOL Multiphysics (the radio frequency module of the frequency-domain study), where the vortex source is generated as the background field.

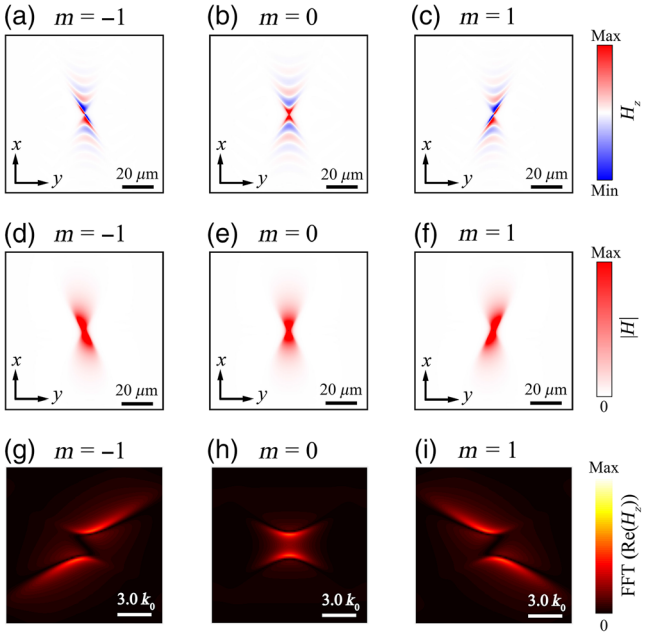

Fig. 1 q-HShPs based on vortex waves with different topological charges ($m = 0, \pm 1$) as excitation sources of hyperbolic materials without off-diagonal permittivity tensor elements at 718 cm^{-1}. (a)–(c) The simulated magnetic fields of different topological charges. (d)–(f) The corresponding intensities ($|H|$) of different topological charges. (g)–(i) The corresponding FFT (Re[H_z]) of different topological charges.

To further demonstrate the phenomena of Fig. 1, we shall prove this in more detail from an analytical perspective. Above all, let us focus on the 2D transverse magnetic polarization, and Maxwell's equations can be described as

$$\begin{cases} \nabla \times \vec{E} = i\omega\mu_0\hat{\mu}\,\vec{H} \\ \nabla \times \vec{H} = -i\omega\varepsilon_0\hat{\varepsilon}\,\vec{E}\,. \end{cases} \tag{1}$$

For the point source in free space, the general solution can be expressed as $H_{\text{point}} = H_m^{(1)}(k_0 r)e^{im\theta}$, where $H_m^{(1)}$ is the m'th-order Hankel function of the first kind, $r = \sqrt{x^2 + y^2}$, $\theta = \arccos(x/r)$ for $y > 0$, and $\theta = 2\pi - \arccos(x/r)$ for $y < 0$. And $m = 0$ is the order of a point source. Likewise, the general solution is appropriate for the vortex waves as excitation sources and m is set as the other nonzero integer values. Considering the anisotropic case, a mapping transformed into an isotropic space can be defined as

$$x = \sqrt{\varepsilon_{vv}}x', \quad y = \sqrt{\varepsilon_{uu}}y', \tag{2}$$

where ε_{uu} and ε_{vv} are the permittivity tensors in a rotated coordinate system $[uvz]$. Therefore, r, θ, and the general solution of hyperbolic materials in the (x', y') coordinate could be rewritten as $r' = \sqrt{\varepsilon_{vv}x'^2 + \varepsilon_{uu}y'^2}$, $\theta' = \arccos(\sqrt{\varepsilon_{vv}}x'/r')$ if $y > 0$, $\theta' = 2\pi - \arccos(\sqrt{\varepsilon_{vv}}x'/r')$ if $y < 0$, and $H_{\text{vortex}} = H_m^{(1)}(k_0 r')e^{im\theta'}$, respectively.[25] Through the derivations, the analytical results excited by different topological charges ($m = \pm 1, \pm 2, \pm 3, \pm 4$) in anisotropic materials at 718 cm^{-1} can be determined, which is appropriate for both cases of hyperbolic and elliptical materials. As shown in Fig. 2, the magnetic fields present the right-skewed q-HShPs for positive topological charges, while negative topological charges stimulate the left-skewed q-HShPs. The asymmetric effect becomes more remarkable as the topological charge increases. Additionally, for odd topological charges, the phase of the upper half differs π from that of the lower half, corresponding to the blue and red part of $m = \pm 1, \pm 3$. In contrast, the phase of the upper half is the same as that of the lower half for even topological charges ($m = \pm 2, \pm 4$), whose magnetic fields present a rotational symmetry distribution and can transform each other (the upper half and lower half) by rotating 180 deg around the origin. Notice that the distribution of the magnetic field near the source, whose patterns are like needles, is associated with the topological charges and changes regularly as the topological charge changes. Our analytical results in Fig. 2 prove a high level of consistency and correctness of the numerical results in Fig. 1. Up to now, the new mechanism of generating q-HShPs by utilizing vortex waves as excitation source has been demonstrated, which is based on the hyperbolic materials without off-diagonal elements and is different from the previous HShPs based on the off-diagonal elements of permittivity tensors.

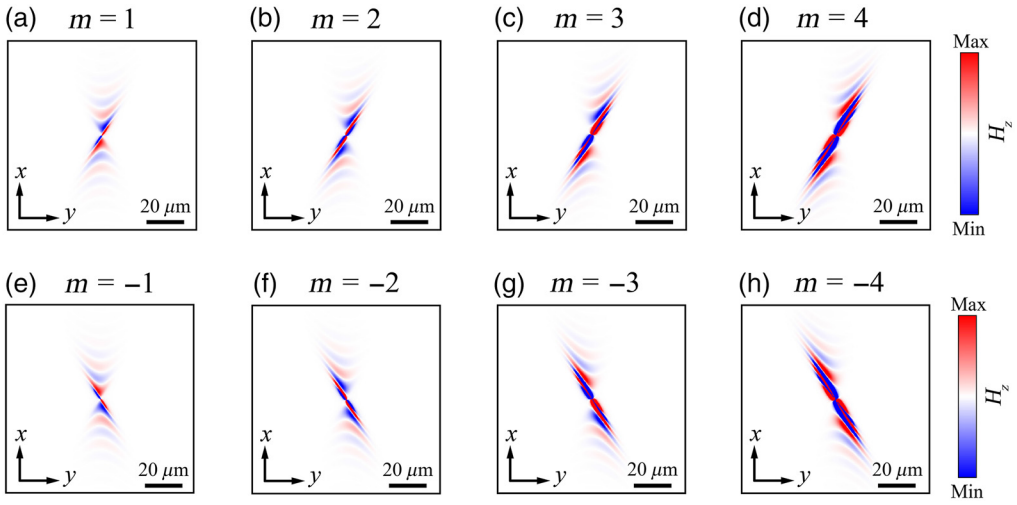

Fig. 2 Analytical results of q-HShPs based on the vortex with different topological charges ($m = \pm1, \pm2, \pm3, \pm4$) as excitation sources of hyperbolic materials without off-diagonal permittivity tensors at 718 cm^{-1}. (a)–(d) The analytical magnetic fields of positive topological charges. (e)–(h) The analytical magnetic fields of negative topological charges.

From the derivation and discussion above, we know that the general solution of vortex waves in anisotropic materials could be denoted as $H_{\text{vortex}} = H_m^{(1)}(k_0 r')e^{im\theta'}$ with $\theta' = \arccos(\sqrt{\varepsilon_{vv}}x'/r)$ for $y > 0$ and $\theta' = 2\pi - \arccos(\sqrt{\varepsilon_{vv}}x'/r)$ for $y < 0$. To better understand the asymmetric phenomenon, we plot the imaginary component of θ' for $\varepsilon_{vv} > 0$ and $\varepsilon_{vv} < 0$ in Fig. 3, respectively, and select $\varepsilon_{uu} = -3 + 0.3i$, $\varepsilon_{vv} = 1 + 0.3i$ and $\varepsilon_{uu} = 3 + 0.3i$, $\varepsilon_{vv} = 1 + 0.3i$ as contrast examples. Because of the existence of negative electric effective tensor elements of hyperbolic materials, θ' has the imaginary component as shown in Fig. 3(a) and $e^{im\theta'}$ becomes a complex number with real and imaginary components. Therefore, for a positive imaginary component [red regions of Fig. 3(a)], $e^{im\theta'}$ becomes an attenuation factor, whereas $e^{im\theta'}$ becomes a gain factor if the imaginary component is negative (blue region), causing the asymmetric q-HShPs. On the contrary, if $\varepsilon_{vv} > 0$,

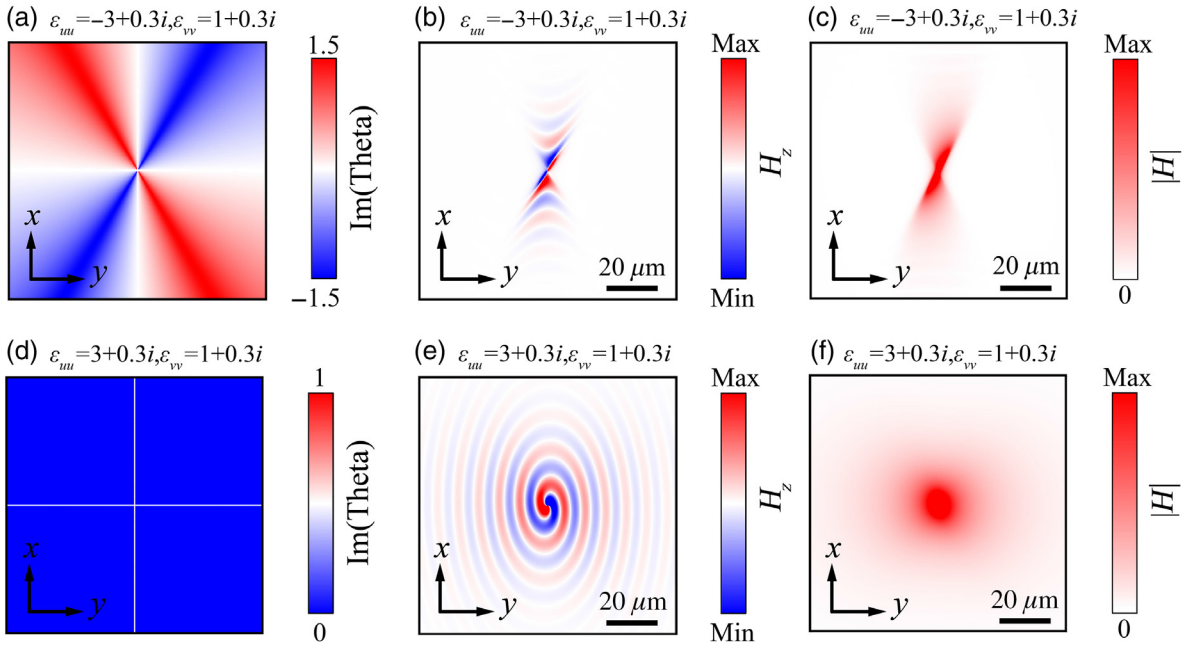

Fig. 3 Explanation of asymmetric q-HShPs in hyperbolic materials. (a) and (d) are the imaginary components of θ' for $\varepsilon_{uu} = -3 + 0.3i$, $\varepsilon_{vv} = 1 + 0.3i$ and $\varepsilon_{uu} = 3 + 0.3i$, $\varepsilon_{vv} = 1 + 0.3i$, respectively. (b) and (e) The corresponding magnetic fields of vortex waves ($m = 1$) as excitation sources at 718 cm^{-1}. (c) and (f) The corresponding intensities of vortex waves ($m = 1$) as excitation sources at 718 cm^{-1}.

the imaginary component of θ' is near to zero [Fig. 3(d)] and the modulus of $e^{im\theta'}$ is identically equal to 1. Based on the analysis above, we plot the magnetic fields and intensities ($|H|$) of $\varepsilon_{vv} < 0$ and $\varepsilon_{vv} > 0$ in Figs. 3(b) and 3(c) and Figs. 3(e) and 3(f), respectively. As we have predicted, for the hyperbolic case ($\varepsilon_{vv} < 0$), the magnetic fields and intensities demonstrate the asymmetric phenomenon [Fig. 3(b) and 3(c)], whereas they become symmetric for the elliptical case ($\varepsilon_{vv} > 0$) [Fig. 3(e) and 3(f)]. These precise and straight analyses not only produce evidence for the generation of asymmetric q-HShPs in hyperbolic materials without off-diagonal elements, but also provide guidance for future exploration of hyperbolic materials.

After demonstrating the generation of q-HShPs in orthogonal systems without off-diagonal elements, we intend to introduce the off-diagonal imaginary component ($\mathrm{Im}(\varepsilon_{uv})$) and explore the propagation characteristics of polaritons excited by vortex sources, as illustrated in Fig. 4, with the permittivity tensors expressed as

$$\begin{pmatrix} \varepsilon_{uu} & i \times f\,\mathrm{Im}(\varepsilon_{uv}) & 0 \\ i \times f\,\mathrm{Im}(\varepsilon_{uv}) & \varepsilon_{vv} & 0 \\ 0 & 0 & \varepsilon_{zz} \end{pmatrix}, \tag{3}$$

where f is the scaling factor for tuning the magnitude of the off-diagonal imaginary component. To measure the asymmetry of the field distributions, we first integrate the modulus of the magnetic field along the dashed red line and blue line ($x = 25\ \mu$m) in Fig. 4(b) at 718 cm^{-1}, respectively, and then calculate the difference between the obtained integral values (the left-hand side minus the right-hand side). The corresponding results for different topological charges m and scaling factors f (corresponding to the horizontal and vertical coordinates) are displayed in Fig. 4(a). The red region in Fig. 4(a) representing the left-skewed q-HShPs shows that the intensity of polaritons propagating along the left is stronger than that of the right, whereas the blue region denotes the right-skewed q-HShPs. The black dashed lines in Fig. 4(a) indicate the critical symmetry transition between the left-skewed q-HShPs and the right-skewed q-HShPs. It is obvious that the symmetry of magnetic fields away from the source can be regulated through tuning the topological charges m and scaling factors f, undergoing the transition of left-skewed q-HShPs to symmetric q-HShPs, and then to right-skewed q-HShPs. Concretely, the symmetric magnetic fields (away from the source) for different topological charges ($m = 0, \pm1, \pm2$) and scaling factors are illustrated in Figs. 4(b)–4(f). As the topological charge m increases, the asymmetrical effect also increases and a larger scaling factor f is needed to return to symmetry. Here a positive scaling factor is required for a positive topological charge to recover as symmetry and vice versa. Compared with the previous generation of HShPs by tuning the scaling factors f, we propose a new mechanism of generating q-HShPs and introduce a new degree of freedom (topological charges m) to control the symmetry (away from the source), which not only possesses the restorability and tunability, but also provides new opportunities for both HShPs and vortex waves to some extent.

To demonstrate the whole transition process, we choose the topological charge $m = 1$ as a specific example in Fig. 5. Compared with the symmetric magnetic field (away from the source) in Fig. 5(b) ($m = 1$, $f = 0.5$), both decreasing and increasing the scaling factor f, the asymmetric effect of q-HShPs will be amplified, exhibiting more distinct left-skewed q-HShPs and right-skewed q-HShPs, as shown in Figs. 5(a) and 5(c) ($f = 1.5$ and $f = -0.5$). Being consistent with the distribution of Fig. 4(a), when raising the scaling factor f, the magnetic fields away from the source will tip to the left side [Fig. 5(a)], corresponding to the red region in Fig. 4(a). And the magnetic fields away from the source will tip to the right side if decreasing the scaling factor f [Fig. 5(c)], corresponding to the blue region in Fig. 4(a). The corresponding intensities ($|H|$) are displayed in Figs. 5(d)–5(f), which demonstrate the asymmetric q-HShPs and present the whole transition process directly.

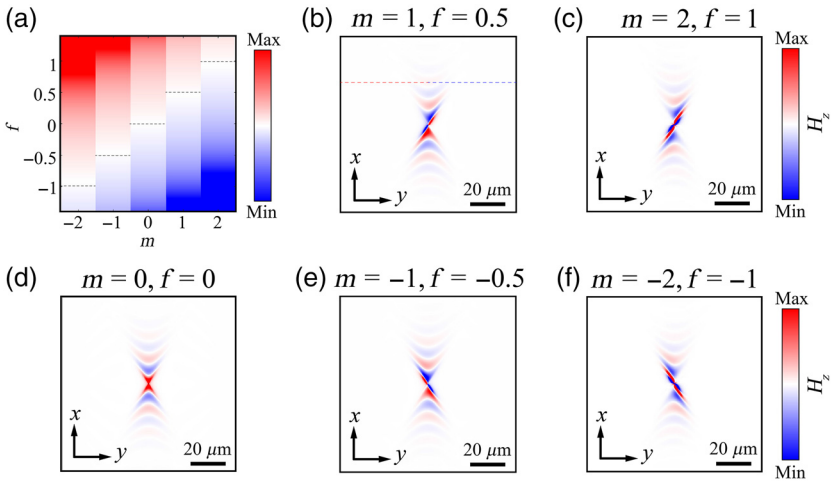

Fig. 4 The critical symmetry transition between the left-skewed and right-skewed q-HShPs induced by the vortex waves at 718 cm^{-1}. (a) The symmetry transition for different topological charges and different scaling factors. (b)–(f) The corresponding symmetric magnetic fields (away from the source) for different topological charges ($m = 0, \pm1, \pm2$) and different scaling factors ($f = 0, \pm0.5, \pm1$) at 718 cm^{-1}, respectively.

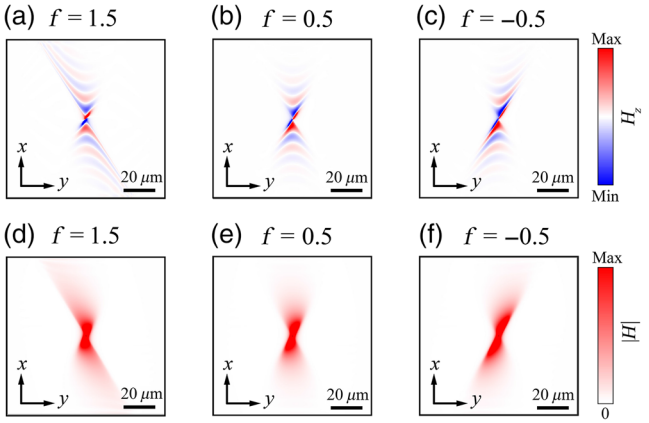

Fig. 5 More distinct asymmetric q-HShPs for decreasing and increasing scaling factors f induced by the vortex waves ($m = 1$) at 718 cm^{-1}. (a)–(c) The magnetic fields of different scaling factors ($f = +1.5, \pm 0.5$). (d)–(f) The corresponding intensities ($|H|$) of different scaling factors ($f = +1.5, \pm 0.5$).

3 Conclusion

In summary, we have proposed an approach to generate q-HShPs and demonstrated its feasibility from both numerical and analytical perspectives. More specifically, if the vortex source is introduced into hyperbolic materials, the q-HShPs will appear in materials without off-diagonal elements and its magnetic fields are related to the parity of topological charges. Moreover, through governing the magnitude of the off-diagonal imaginary components and topological charges, the symmetry of magnetic fields away from the source can be tuned, which offers a restorable and tunable way for future research on q-HShPs. It should be noted that our work provides a degree of freedom for tuning the q-HShPs and vortex waves, which has tremendous promise for implementation and expansion in other sources, such as Janus and Huygens dipoles.[26]

Acknowledgments

This work is supported by the National Natural Science Foundation of China (Grant Nos. 92050102 and 11904006); The National Key Research and Development Program of China (Grant No. 2020YFA0710100); Jiangxi Provincial Natural Science Foundation (Grant Nos. 20224ACB201005); Shenzhen Science and Technology Program (Grant Nos. JCYJ20210324121610028) and the Fundamental Research Funds for the Central Universities (Grant Nos. 20720200074, 20720220134, and 20720220033).

References

1. H. Raether, Ed., "Surface plasmons on smooth surfaces," in *Surface Plasmons on Smooth and Rough Surfaces and on Gratings*, pp. 4–39, Springer (1988).
2. S. A. Maier, Ed., "Surface plasmon polaritons at metal/insulator interfaces," in *Plasmonics: Fundamentals and Applications*, pp. 21–37, Springer (2007).
3. D. K. Gramotnev and S. I. Bozhevolnyi, "Plasmonics beyond the diffraction limit," *Nat. Photonics* **4**(2), 83–91 (2010).
4. H. A. Atwater and A. Polman, "Plasmonics for improved photovoltaic devices," *Nat. Mater.* **9**, 205–213 (2010).
5. Q. Zhang et al., "Interface nano-optics with van der Waals polaritons," *Nature* **597**, 187 (2021).
6. D. Lee et al., "Hyperbolic metamaterials: fusing artificial structures to natural 2D materials," *eLight* **2**, 1 (2022).
7. S. Dai et al., "Tunable phonon polaritons in atomically thin van der Waals crystals of boron nitride," *Science* **343**(6175), 1125–1129 (2014).
8. J. D. Caldwell et al., "Sub-diffractional volume-confined polaritons in the natural hyperbolic material hexagonal boron nitride," *Nat. Commun.* **5**(1), 1–9 (2014).
9. J. D. Caldwell et al., "Photonics with hexagonal boron nitride," *Nat. Rev. Mater.* **4**(8), 552–567 (2019).
10. W. Ma et al., "In-plane anisotropic and ultra-low-loss polaritons in a natural van der Waals crystal," *Nature* **562**(7728), 557–562 (2018).
11. Z. Zheng et al., "A midinfrared biaxial hyperbolic van der Waals crystal," *Sci. Adv.* **5**(5), eaav8690 (2019).
12. Z. Zheng et al., "Highly confined and tunable hyperbolic phonon polaritons in van der Waals semiconducting transition metal oxides," *Adv. Mater.* **30**(13), 1705318 (2018).
13. Z. Dai et al., "Edge-oriented and steerable hyperbolic polaritons in anisotropic van der Waals nanocavities," *Nat. Commun.* **11**(1), 1–8 (2020).
14. G. Hu et al., "Topological polaritons and photonic magic angles in twisted α-MoO_3 bilayers," *Nature* **582**(7811), 209–213 (2020).
15. N. Passler et al., "Hyperbolic shear polaritons in low-symmetry crystals," *Nature* **602**(7898), 595–600 (2020).
16. A. Ashkin, "Acceleration and trapping of particles by radiation pressure," *Phys. Rev. Lett.* **24**, 156–159 (1970).
17. M. Padgett and R. Bowman, "Tweezers with a twist," *Nat. Photonics* **5**, 343–348 (2011).
18. J. Wang et al., "Terabit free-space data transmission employing orbital angular momentum multiplexing," *Nat. Photonics* **6**, 488–496 (2012).
19. S. Fürhapter et al., "Spiral phase contrast imaging in microscopy," *Opt. Express* **13**, 689–694 (2005).
20. F. Tamburini et al., "Overcoming the Rayleigh criterion limit with optical vortices," *Phys. Rev. Lett.* **97**, 163903 (2006).
21. K. Dholakia et al., "Second-harmonic generation and the orbital angular momentum of light," *Phys. Rev. A* **54**, R3742–R3745 (1996).
22. J. Courtial et al., "Second-harmonic generation and the conservation of orbital angular momentum with high-order Laguerre-Gaussian modes," *Phys. Rev. A* **56**, 4193–4196 (1997).
23. L. Xiong et al., "Polaritonic vortices with a half-integer charge," *Nano Lett.* **21**, 9256 (2021).
24. M. Wang et al., "Spin-orbit-locked hyperbolic polariton vortices carrying reconfigurable topological charges," *eLight* **2**, 12 (2022).
25. S. Tao et al., "Anisotropic Fermat's principle for controlling hyperbolic van der Waals polaritons," *Photonics Res.* **10**, B14–B22 (2022)
26. M. F. Picardi, A. V. Zayats, and F. J. Rodríguez-Fortuño, "Janus and Huygens dipoles: near-field directionality beyond spin-momentum locking," *Phys. Rev. Lett.* **120**, 117402 (2018).